Phys Chem Minerals (1998) 26:83–99

ORIGINAL PAPER

J.A. Tangeman · R.A. Lange

The effect of Al^{3+}, Fe^{3+}, and Ti^{4+} on the configurational heat capacities of sodium silicate liquids

Received: 18 July 1997/ Revised, accepted: 18 June 1998

Abstract The heat capacities of 29 glasses and supercooled liquids in the Na_2O-SiO_2, Na_2O-Al_2O_3-SiO_2, Na_2O-(FeO)-Fe_2O_3-SiO_2, and Na_2O-TiO_2-SiO_2 systems were measured in air from 328 to 998 K with a differential scanning calorimeter. The reproducibility of the data determined from multiple heat capacity runs on a single crystal MgO standard is within ± 1% of the accepted values at temperatures ≤ 800 K and within ± 1.5% between 800 and 1000 K. Within the resolution of the data, the heat capacities of sodium silicate and sodium aluminosilicate liquids are temperature independent. Heat capacity data in the supercooled liquid region for the sodium silicates and sodium aluminosilicates were combined and modelled assuming a linear compositional dependence. The derived values for the partial molar heat capacities of Na_2O, Al_2O_3, and SiO_2 are 112.35 ± 0.42, 153.16 ± 0.82, and 76.38 ± 0.20 J/gfw · K respectively. The partial molar heat capacities of Fe_2O_3 and TiO_2 could not be determined in the same manner because the heat capacities of the Fe_2O_3- and TiO_2-bearing sodium silicate melts showed varying degrees of negative temperature dependence. The negative temperature dependence to the configurational C_P may be related to the occurrence of submicroscopic domains (relatively polymerized and depolymerized) that break down to a more homogeneous melt structure with increasing temperature. Such an interpretation is consistent with data from *in situ* Raman, Mössbauer, and X-ray absorption fine structure (XAFS) spectroscopic studies on similar melts.

J.A. Tangeman[1] (✉) · R.A. Lange
University of Michigan, Department of Geological Sciences,
2534 C. C. Little Building, 425 E. University Ave., Ann Arbor,
MI 48109-1063, USA
e-mail: jatangeman@ucdavis.edu

Present address:
[1] University of California, Davis, Thermochemistry Facility,
Chemistry Building,
Department of Chemical Engineering and Materials Science,
Davis, CA 95616-8779, USA
Phone: +1-530-754-2132
Fax: +1-530-752-9307

Key words heat capacity · silicate glasses · glass transition · silicate liquids · configurational heat capacity

Introduction

The success of using thermodynamic data to calculate mineral-liquid phase equilibria is dependent upon accurate values of the enthalpy and entropy of silicate liquids which, in turn, require accurate determination of liquid heat capacities as a function of temperature and composition. Both vibrational and configurational components contribute to the heat capacity of silicate liquids:

$$C_P^{liq}(T) = C_P^{conf}(T) + C_P^{vib}(T) \quad (1)$$

where C_P^{vib} is the vibrational contribution and C_P^{conf} is the configurational contribution to the liquid heat capacity at temperatures above the glass transition. The configurational heat capacity reflects changes in melt structure that occur with temperature and thus provides a quantitative link between thermodynamic and transport properties, such as viscosity. Previous studies on alkali titanosilicate melts show anomalously large configurational heat capacities at the glass transition temperature (T_g) (Richet and Bottinga 1985; Lange and Navrotsky 1993). Above T_g, the heat capacities of the melts decrease with temperature. Based on an *in situ* high-temperature Ti K-edge XAFS spectroscopic study, Farges et al. (1996c) suggested that the anomalous variations in the heat capacities of Na- and K-titanosilicate melts are related to the occurrence of $^{[5]}Ti^{4+}$ along the interface of alkali-rich and network former-rich domains and the breakdown of these domains at temperatures above T_g. The goal of this study was to directly measure the configurational heat capacity of liquids in the Na_2O-SiO_2, Na_2O-Al_2O_3-SiO_2, Na_2O-(FeO)-Fe_2O_3-SiO_2, and Na_2O-TiO_2-SiO_2 systems and to evaluate the magnitude of the effects of the network-forming cations (Al^{3+}, Fe^{3+}, and Ti^{4+}) on the configurational heat capacities of the sodium silicate liquids. The sodium silicate

liquids serve effectively as an 'end-member' system for the other three ternary silicate systems.

The low glass transition temperatures of samples in the four systems permitted direct measurement of the heat capacity of the supercooled liquids with a differential scanning calorimeter (Perkin-Elmer DSC-7). The DSC is ideal for quantitative assessment of the configurational contribution to the liquid heat capacity because measurements of low-temperature liquid heat capacities (≤ 1000 K) are performed directly and the glass transition can be scanned through continuously, with a reproducibility of 1–2%. In addition, the heat capacities observed for the sodium silicate glasses and supercooled liquids in this investigation are compared to heat capacity data for sodium silicate glasses and the corresponding supercooled and stable liquids reported in the literature (Richet et al. 1984; Knoche et al. 1994). Such a comparison provides an assessment of interlaboratory accuracy for this well studied system at temperatures above and below the glass transition.

Experimental methods

Sample synthesis and composition analyses

Ten of the 29 glasses investigated in this study were previously synthesized by others. These include six Na_2O-Al_2O_3-SiO_2 glasses (NAS-2, -8, -9, -10, -15, -B; Stein et al. 1986), one Na_2O-(FeO)-Fe_2O_3-SiO_2 glass (acmite; Lange and Carmichael 1987), and three Na_2O-TiO_2-SiO_2 glasses (LC-20; Lange and Carmichael 1987; NTS-1 and –5; Johnson and Carmichael 1987). These ten samples were remelted at 1473–1823 K to drive off any absorbed water and then were analyzed with a Cameca Camebax electron microprobe at the University of Michigan to confirm that no measurable change in composition had occurred during the re-fusion process.

The remaining 19 samples in the Na_2O-SiO_2, Na_2O-(FeO)-Fe_2O_3-SiO_2, and Na_2O-TiO_2-SiO_2 systems were prepared from appropriate proportions of reagent grade Na_2CO_3, Fe_2O_3, TiO_2 and SiO_2. The amount of water absorbed by each of the reagents was determined by weighing before and after drying in a furnace and then subtracted when calculating the proportions of each undried reagent to be mixed. Sample batches of ~200 grams were mixed by manually shaking in a glass jar for several minutes. The mixed powders were then dried and decarbonated at 1073 K and fused in a platinum crucible at 1373 K. The samples were quenched to a glass, ground to a powder and re-fused; to ensure homogeneity, this procedure was repeated at least twice. To minimize the reduction of Fe_2O_3 to FeO, all steps in the fusion process were carried out in air and the fusions were performed at temperatures <1373 K (except for NFS-8 and acmite, whose higher liquidus temperatures required that they be fused at temperatures approaching 1473 K). Although a relatively minor amount of iron (Fe^{2+}) loss to the platinum may occur at the higher temperatures of the synthesis procedure, it is not considered a problem because the sample compositions were determined after the fusions.

Concentrations of Na_2O, Al_2O_3, total Fe_2O_3, TiO_2, and SiO_2 in the sample glasses were determined by I. S. E. Carmichael (U. C. Berkeley) using wet chemical methods. The analyses were performed before the heat capacity runs. For samples in the Na_2O-(FeO)-Fe_2O_3-SiO_2 system, wet chemical analyses of FeO were performed at the University of Michigan following the procedure of Wilson (1960). Most samples had ≤0.40 wt % FeO (Table 1). Because of such low concentrations of ferrous iron, the Na_2O-(FeO)-Fe_2O_3-SiO_2 system is effectively considered a ternary system in this investigation. However, for the sake of accurately representing the system, FeO is shown parenthetically. The iron-bearing glasses were

Table 1 Wet chemical analyses of experimental liquids (wt.%)

Sample	Na_2O	Al_2O_3	Fe_2O_3	FeO	TiO_2	SiO_2	Total
NS-1	22.34	–	–	–	–	77.85	100.19
NS-2	26.30	–	–	–	–	73.81	100.11
NS-3	32.16	–	–	–	–	67.85	100.01
NS-4	35.86	–	–	–	–	64.50	100.36
NS-5	40.00	–	–	–	–	59.21	99.21
NS-6	47.90	–	–	–	–	52.60	100.50
NS-7	53.02	–	–	–	–	47.37	100.39
NAS-2	19.54	17.59	–	–	–	62.63	99.76
NAS-8	32.57	9.73	–	–	–	57.31	99.61
NAS-9	25.20	19.73	–	–	–	55.39	100.32
NAS-10	22.44	24.43	–	–	–	52.88	99.75
NAS-15	29.88	23.06	–	–	–	46.89	99.83
NAS-B	16.92	12.33	–	–	–	70.60	99.85
NFS-1	30.32	–	36.31	0.28	–	32.09	99.00
NFS-2	31.64	–	26.51	0.32	–	41.11	99.57
NFS-3	33.00	–	16.12	0.30	–	49.90	99.33
NFS-4	28.15	–	21.50	0.40	–	50.42	100.47
NFS-5	28.29	–	10.51	0.26	–	61.15	100.21
NFS-6	22.03	–	19.58	0.29	–	57.55	99.45
NFS-7	24.68	–	3.55	0.21	–	71.26	99.70
NFS-8	10.51	–	21.00	0.65	–	66.97	99.13
Acmite	13.25	–	32.68	1.44	–	52.37	99.74
NTS-1	28.51	–	–	–	12.49	58.64	99.64
NTS-2	22.89	–	–	–	30.48	46.07	99.44
NTS-3	25.44	–	–	–	12.47	61.45	99.36
NTS-4	31.58	–	–	–	32.78	35.92	100.28
NTS-5	31.89	–	–	–	39.86	28.18	99.93
NTS-6	13.07	–	–	–	33.14	53.08	99.29
LC-20	25.50	–	–	–	19.34	54.73	99.57

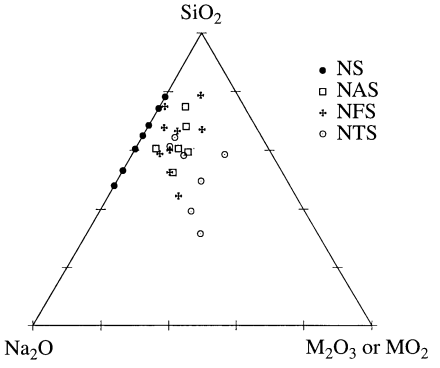

Fig. 1 Plot of glass compositions within the Na_2O-SiO_2-MO_2 or M_2O_3 ternary system (mol %). *Solid circles* represent samples in the Na_2O-SiO_2 system; *open squares*, Na_2O-Al_2O_3-SiO_2 system; *crosses*, Na_2O-Fe_2O_3(total)-SiO_2 system; *open circles*, Na_2O-TiO_2-SiO_2 system

not taken to temperatures above 1273 K during the heat capacity runs or pre-run heat treatments. Once NFS-8 and acmite were synthesized at temperatures around 1473 K, they underwent no further heat treatment in addition to the C_P runs. The FeO contents at temperatures <1273 K are expected to be ≤ 0.2 wt. % and therefore negligible (Lange and Carmichael 1989). The analyses of the glasses are given in Table 1 and shown in Fig. 1.

Sample loading and heat treatment

Between 48 and 52 mg of each sample in the Na_2O-Al_2O_3-SiO_2, Na_2O-(FeO)-Fe_2O_3-SiO_2, and Na_2O-TiO_2-SiO_2 systems were loaded into gold pans, crimped shut and stored in a desiccator. Immediately prior to each heat capacity run, the gold-encased sample was placed in a Pt crucible and then heated in a box furnace in air to approximately 50 degrees above its melting temperature (which was at or below 1273 K), held for ~5 min at that temperature, and then the bottom of the Pt crucible was immersed in cold water so as to quench the sample liquid to glass, thus preventing crystallization. Except for NFS-8 and acmite, whose liquidus temperatures exceeded that of the melting temperature of gold (1336 K), all other glass samples were treated in this manner before each heat capacity run. (NFS-8 and acmite were simply cycled through the DSC with no pre-melting treatment prior to the experimental runs.) Thus, even though a sample underwent repeated DSC heating runs, the starting material for each experimental run was always a glass because of the 're-melting and quenching' treatment. For some samples (e.g., NTS-5 and the majority of the sodium silicates) crystallization occurred during the DSC run at high temperatures so that liquid data were available only for the lower temperature portion of the supercooled liquid region. In these cases, the onset of crystallization was marked by a precipitous drop in the measured heat capacity.

Samples in the Na_2O-SiO_2 binary were treated somewhat differently because of their hygroscopic nature and their tendency to crystallize above T_g. Before each run, a few grams of the homogenized sample stock was rapidly re-fused (typically in less than 10 min, thus minimizing the possibility of Na volatilization) and then quenched in water. The freshly remelted and quenched sample was then coarsely crushed and 48–52 mg samples were loaded into the gold pans. The crushing and loading were performed in an atmosphere of dry air. After loading and weighing, the sample was placed directly into the DSC. Because most of the Na_2O-SiO_2 samples crystallized by the end of a DSC heating run, a 'fresh' sample was loaded into the cleaned gold pan using the procedure just described before a new run. Significant Na volatilization is not expected to have occurred during the experiment because the temperature maximum for all samples was less than 1003 K and the duration of the DSC scans above T_g was at most one hour.

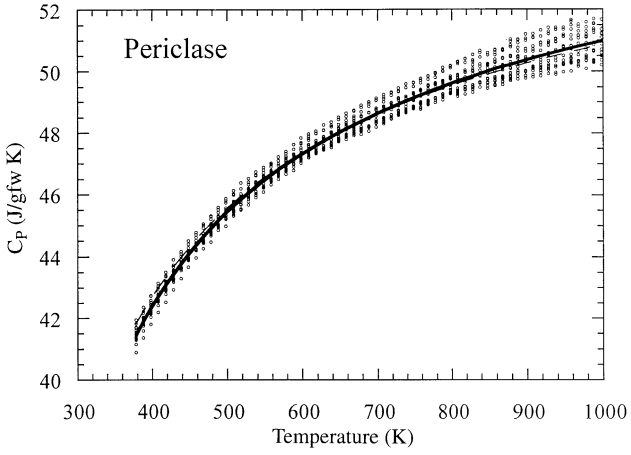

Fig. 2 Experimental heat capacity runs for periclase (MgO). *Solid line* represents curve fitted through 17 experimental runs using equation of the form: $a + bT + cT^{-2} + dT^{1/2} + eT^2$. *Dashed line* represents fitted curve of Robie and Hemingway (1995) for periclase

Calorimetric techniques and data reduction

A power compensated differential scanning calorimeter (Perkin-Elmer DSC-7) was used to measure the heat capacities of the 29 samples. Measurements for all samples were performed in an atmosphere of dry air flowing at a rate of 30 cc/min. The known melting points of indium (429.75 K) and zinc (692.55 K) were used for temperature calibration. To maintain stable temperatures, a turbulent chamber through which a constant flow of chilled water (~45–50 °C) circulated was attached to the calorimeter block. A typical DSC heat capacity experiment consisted of ten degree scans of the baseline (empty Au pan with Au lid), ~50 mg of the pure corundum (Al_2O_3) NBS-720 standard encased in gold, and one to five samples over a 373–1003 K temperature range. To begin an experiment, the calorimeter was loaded with the empty Au pan and held at 373 K until thermal equilibrium was attained. A ten degree temperature interval was then scanned with a heating rate of 10 K/min and held at the end temperature of the interval for one minute. The end temperature of the scanned interval was then used as the starting temperature for the next ten degree scan. It was determined that one minute was sufficient for the milliwatt reading to stabilize before the beginning of the next ten degree scan. This method of step scanning was used instead of continuous scanning in order to minimize instrumental drift and thus increase the accuracy of the results (Lange and Navrotsky 1993). This procedure was used throughout the 630 degree temperature range and was used for the standard and sample runs as well as the baseline; the duration of each run was about three hours. Thus, in 9 h (3 h/baseline run, 3 h/standard run, and 3 h/sample run), a complete heat capacity curve for one unknown from 373 K to 1000 K could be generated. Typically, up to four samples per day were run using the same baseline and standard data.

Results for each sample run were calibrated against the measurement of the NBS-720 standard in conjunction with data on pure Al_2O_3 (Ditmars and Douglas 1971). The heat capacities of the unknown samples were then calculated using an algorithm based on the method of Mraw (1988). Corrections for differences in pan weights, up to 9.33 mg, were made using the C_P for gold (Robie and Hemingway 1995). The heat capacity values plotted in Figs. 2–7 for each sample are those taken five degrees above the start of each ten degree temperature interval.

Inter- and intralaboratory errors

During the period of time over which heat capacity experiments were performed on the 29 samples, 17 heat capacity curves on a single

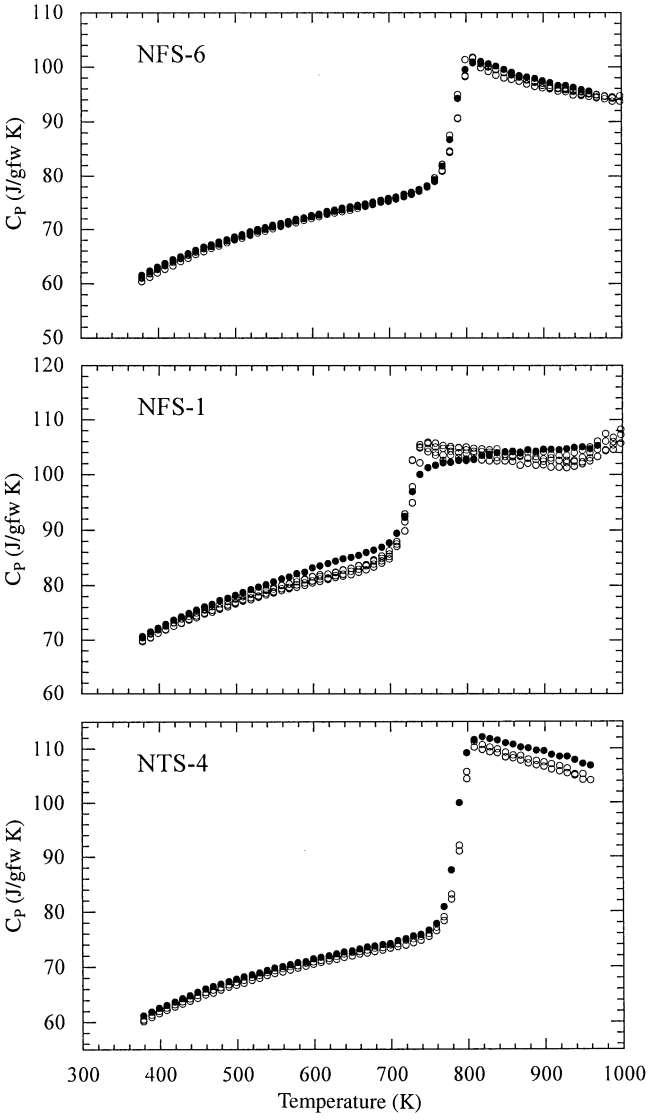

Fig. 3 Reversal data for NFS-6, NFS-1, and NTS-4. *Open circles* represent experimental data for DSC heating runs; *solid filled circles* represent cooling runs

crystal of periclase (MgO; 50 mg) were generated as well. The MgO was run in the same manner as the samples and was periodically included as a sample during a daily experiment. The periclase is an inter- and intralaboratory standard (Bosenick et al. 1996). All 17 curves (shown as sequences of open circles) are plotted in Fig. 2 along with the fitted curve (solid line) which incorporates all of the data and the curve of Robie and Hemingway (1995) (dashed line). The agreement between the fitted curve and that of Robie and Hemingway (1995) is excellent, the maximum discrepancy being 0.8%.

The C_P data of Bosenick et al. (1996) on a sample of the same batch of MgO were compared to the curve fitted to the experimental data of this study. The averages of the heat capacities of Bosenick et al. (1996) are slightly higher than our fitted curve for temperatures in the range 330–970 K. However, the discrepancy is generally less than 0.4% and approaches but does not exceed 1.0% at only the highest temperatures.

Calorimetric test for equilibrium

To ascertain whether or not the heat capacity measurements at temperatures above T_g were equilibrium measurements, reversal heat capacity runs were performed on representative samples in the sodium iron silicate and sodium titanosilicate system (Fig. 3). For the reversal runs, the samples were first heated to 1003 K in the calorimeter and then held at that temperature until the milliwatt reading stabilized (~5 min). Following this, the heat capacities of the samples were measured in ten degree step scans at a cooling rate of ten degrees/min. The heating curves for NFS-6 and NTS-4 are equivalent to their respective cooling curves (Fig. 3), indicating that the samples are at equilibrium and that the observed temperature dependence in these samples is real and not likely a result of incipient crystallization. In contrast, the disagreement between the cooling and heating curves for NFS-1 indicates that a non-equilibrium phenomenon is occurring. Indeed, when the 'post-DSC run' sample of NFS-1 was removed from its gold pan and ground to a thin wafer, a few crystals were visible when the wafer was held up to the light.

Results

Glasses

Heat capacity data for the glasses and supercooled liquids in the temperature range 328–998 K for the 29 samples are presented in Figs. 4–7. The heat capacity curves for the Na_2O-SiO_2 system are presented, followed by the Na_2O-Al_2O_3-SiO_2, Na_2O-(FeO)-Fe_2O_3-SiO_2, and Na_2O-TiO_2-SiO_2 systems. Within each system, the sample C_P curves are presented in order of increasing glass transition temperatures. For each figure, open circles represent experimental runs made on different days. The heat capacity data for the 29 individual glasses were fitted to a three term Maier-Kelley equation ($C_P = a + bT + cT^{-2}$; Table 2) which is shown in Figs. 4–7 by the solid curve. The glass data to which the curves are fitted can be found in Tangeman (1998).

Models such as those of Stebbins et al. (1984) and Richet (1987) predict glass heat capacities as a function of temperature and composition. These models assume that the partial molar heat capacities are independent of composition. Because the heat capacity of silicate glasses is due primarily to interatomic vibrations which are insensitive to local structure above room temperature, this assumption is justified. These models employ the Maier-Kelley expression to describe the temperature dependence of the heat capacities. This expression suffices since extrapolations to high temperatures are not necessary given that glass transition temperatures are generally lower than the melting temperatures of crystalline equivalents. Typically, the models of Stebbins et al. (1984) and Richet (1987) recover measured data upon which they are calibrated to within ± 1%. However, the model of Richet (1987) is calibrated on a wider compositional and temperature range of data. In Figs. 4–7, a comparison is made between our measured glass heat capacities and those calculated from Richet (1987) (represented by the dashed curve).

For the seven sodium silicates, the model curve of Richet (1987) is higher than the experimental data of this study, but converges and then crosses over as temperatures approach the glass transition. Agreement of the sodium silicate glass data with the model values is

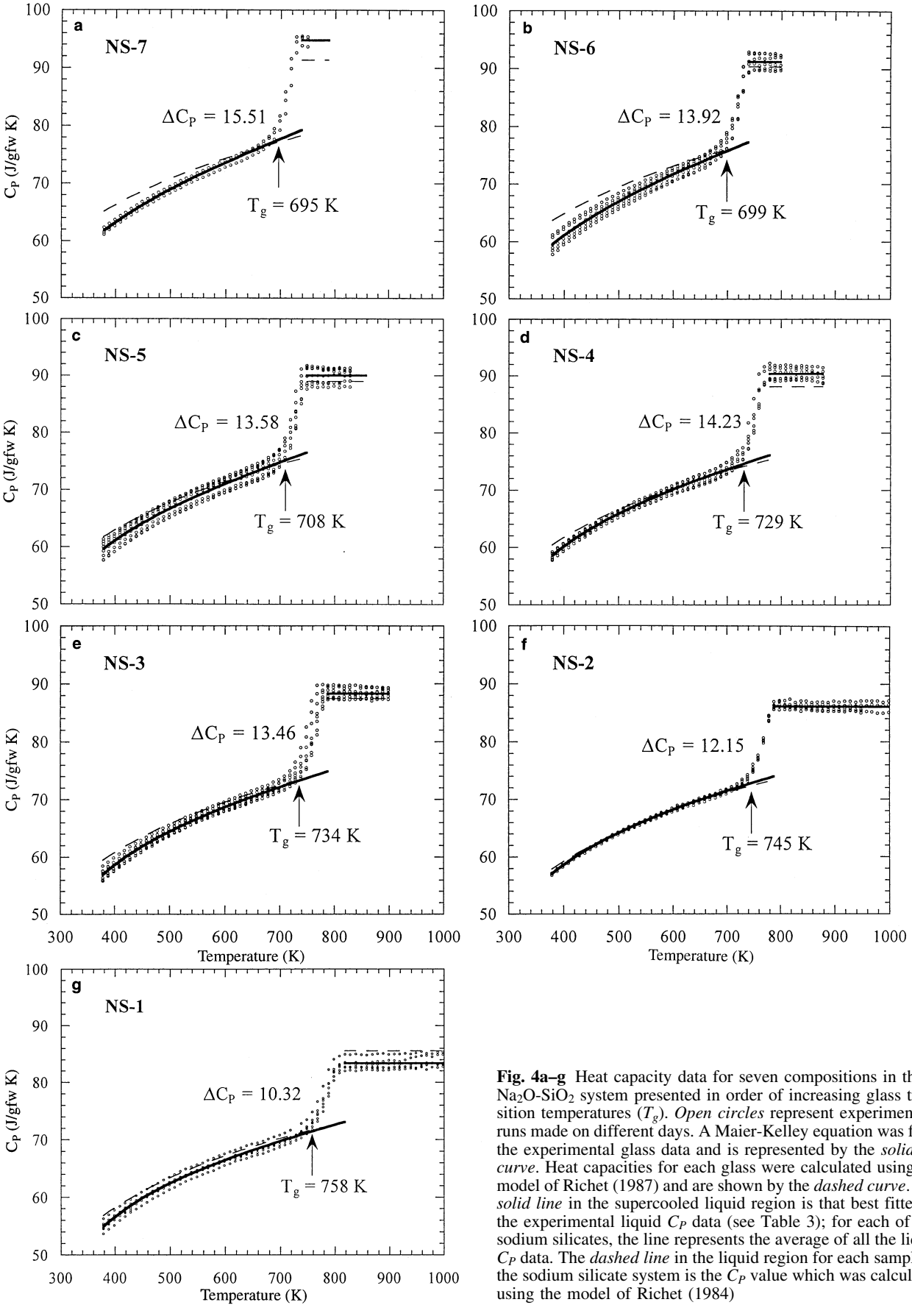

Fig. 4a–g Heat capacity data for seven compositions in the Na_2O-SiO_2 system presented in order of increasing glass transition temperatures (T_g). *Open circles* represent experimental runs made on different days. A Maier-Kelley equation was fit to the experimental glass data and is represented by the *solid curve*. Heat capacities for each glass were calculated using the model of Richet (1987) and are shown by the *dashed curve*. The *solid line* in the supercooled liquid region is that best fitted to the experimental liquid C_P data (see Table 3); for each of the sodium silicates, the line represents the average of all the liquid C_P data. The *dashed line* in the liquid region for each sample in the sodium silicate system is the C_P value which was calculated using the model of Richet (1984)

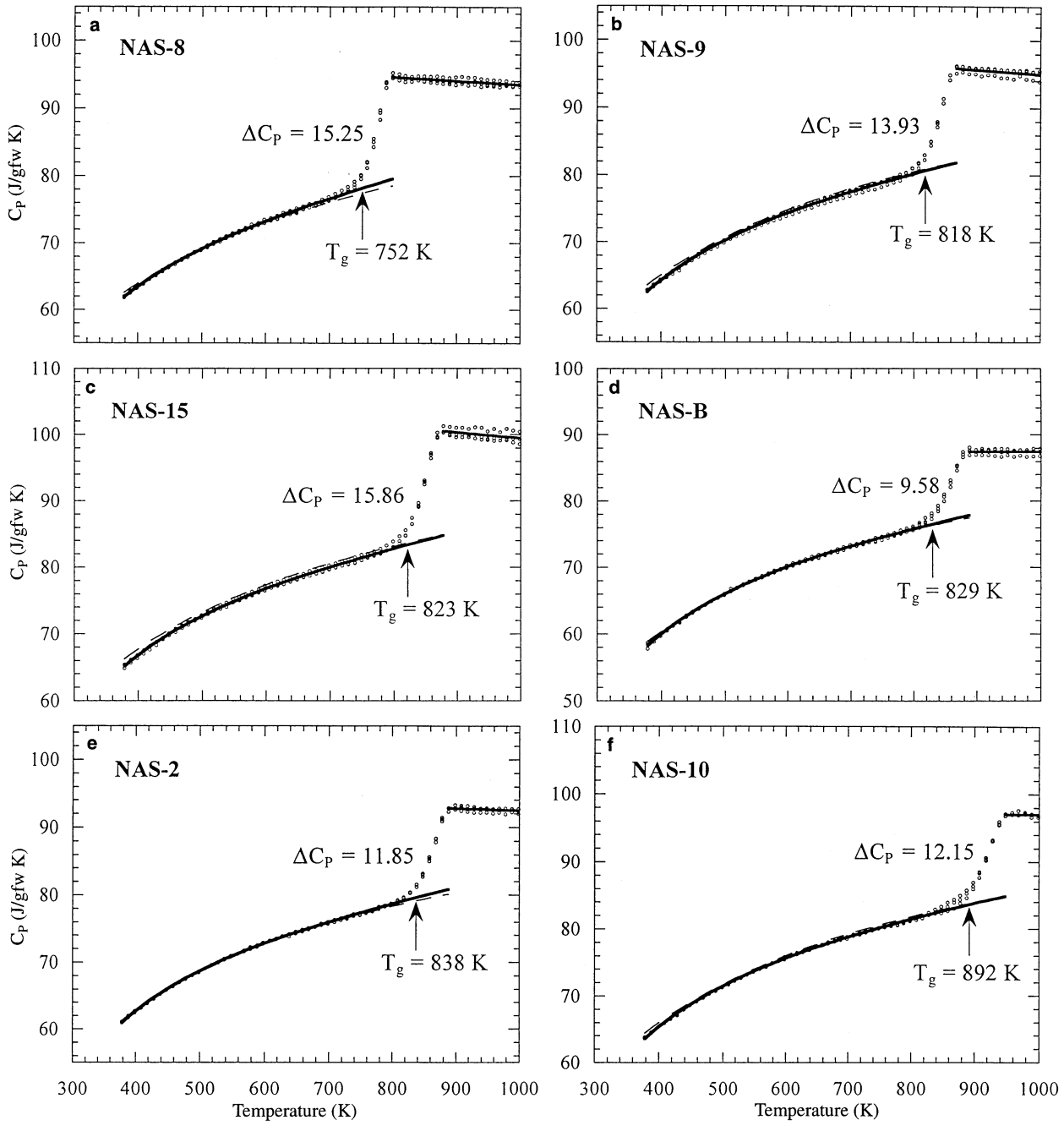

Fig. 5a–f Heat capacity data for six compositions in the Na_2O-Al_2O_3-SiO_2 system. Description of the details of each diagram are as in Fig. 4

poorest at the lowest temperatures. One of the main factors contributing to discrepancies between the model and experimental curves is that the model of Richet (1987) is calibrated on glasses with Na_2O contents between 0 and 33 mol%, whereas the glasses of this study range up to 52 mol% Na_2O. In addition, adiabatic calorimetry data indicate that the heat capacities of sodium silicate glasses are not quite additive functions of composition near room temperature (P Richet, personal communication). Model glass curves for the aluminum- and most of the iron-bearing sodium silicates are in close agreement with the individual fitted curves for the experimental runs because the model of Richet (1987) is suitably calibrated for these compositions. The model curves for nearly all of the sodium titanosilicates, on the other hand, are significantly higher than the individual fitted curves, especially at temperatures approaching T_g. The deviation is most pronounced for the samples whose TiO_2 concentration (NTS-2, -4, -5, -6) is outside the range of TiO_2 contents on which the model is calibrated (0–17 mol%).

Table 2 Equations fitted to the heat capacities of individual glasses ($C_P=a+bT+c/T^2$) with corresponding glass transition temperatures and configurational heat capacities (J/gfw K)

Sample	Number of runs	a	$b\times10^2$	$c\times10^{-5}$	SE estimation	T_{max} (K)	T_g (K)	C_P^{conf} (T_g)	% C_P^{conf}
NS-1	6	59.051	2.0214	–16.830	0.68	738	758	10.32	1.40
NS-2	5	59.712	2.1218	–15.284	0.23	708	745	12.15	1.72
NS-3	8	59.091	2.3214	–15.619	0.71	708	734	13.46	1.90
NS-4	6	59.484	2.4465	–14.542	0.62	698	729	14.32	2.04
NS-5	8	57.153	2.8679	–12.030	1.13	688	708	13.58	1.97
NS-6	6	55.239	3.2797	–11.542	0.98	678	699	13.92	2.05
NS-7	3	55.906	3.4155	–10.089	0.49	668	695	15.51	2.32
NAS-2	3	67.039	1.8178	–18.535	0.13	808	838	11.85	1.47
NAS-8	3	63.499	2.3026	–14.738	0.21	718	752	15.25	2.12
NAS-9	3	68.382	1.8323	–18.224	0.29	778	818	13.93	1.79
NAS-10	3	70.746	1.7213	–19.601	0.13	838	892	12.15	1.45
NAS-15	3	69.718	1.9727	–17.249	0.28	788	823	15.86	2.01
NAS-B	3	65.490	1.6694	–19.372	0.19	798	829	9.58	1.20
NFS-1	4	73.565	1.9910	–15.632	0.42	668	703	20.07	3.00
NFS-2	3	65.360	2.7289	–12.467	0.23	668	706	19.41	2.91
NFS-3	3	60.923	2.9168	–11.696	0.17	668	707	20.69	3.10
NFS-4	2	63.413	2.4611	–12.892	0.13	698	730	22.82	3.27
NFS-5	2	61.442	2.2147	–15.816	0.20	708	753	19.31	2.73
NFS-6	4	65.103	1.9979	–16.589	0.27	718	768	23.05	3.21
NFS-7	2	59.482	2.2642	–14.815	0.26	728	757	15.17	2.08
NFs-8	2	66.900	1.3936	–20.845	0.18	778	805	9.76	1.25
Acmite	4	68.707	2.0756	–17.255	0.43	738	773	14.40	1.95
NTS-1	2	62.200	1.8902	–15.665	0.22	768	802	21.09	2.75
NTS-2	2	65.216	1.3493	–16.864	0.15	798	850	35.09	4.40
NTS-3	2	63.066	1.6389	–17.260	0.11	778	813	20.32	21.32
NTS-4	2	64.115	1.8206	–15.071	0.27	728	772	34.27	30.93
NTS-5	2	63.584	1.8961	–12.574	0.26	738	780	42.58	5.77
NTS-6	2	64.684	1.2541	–19.215	0.22	848	888	28.43	3.35
LC-20	2	63.548	1.6323	–16.090	0.21	778	830	27.54	3.54

Supercooled liquids

Sodium silicates

Heat capacity data for the sodium silicate liquids are shown in Fig. 4a-g, and the number of individual runs for each sample is shown in Table 2. The average values for the liquid heat capacities of the seven samples are given in Table 3 and shown in Fig. 4a-g as a solid horizontal line above T_g. The complete C_P data sets for the sodium silicate liquids and for the Al-, Fe-, and Ti-bearing liquids are in Tangeman (1998). The hygroscopic nature of the sodium silicates and their tendency to crystallize in the supercooled liquid field necessitated loading a freshly re-melted and quenched glass sample prior to each run, which contributed to the greater scatter among the sodium silicate heat capacity curves relative to the Al-, Fe-, and Ti-bearing samples. Therefore, more scans were performed on the sodium silicates than the other samples in an effort to improve the accuracy of the C_P determinations. Within error, no temperature dependence to the liquid C_P could be resolved for the sodium silicates. In general, as the glass transition temperature decreases, the configurational heat capacity at the glass transition temperature, $C_P^{conf}(T_g)$, increases and the temperature range over which liquid data are accessible (before crystallization) decreases. The heat capacities of the sodium silicate liquids in this study agree to within 2.5% of the values calculated using the model of Richet et al. (1984) (shown as dashed line at $T>T_g$ in Fig. 4a–g) and to within 3.5% of the experimental data of Knoche et al. (1994).

Sodium aluminosilicates

For each of the sodium aluminosilicates, three runs were performed and the reproducibility is excellent (Fig. 5a-f). For NAS-10 and NAS-B, the heat capacity data for the supercooled liquid are constant with temperature. For the remaining four sodium aluminosilicates (NAS-2, -8, -9, and –15), the line that most accurately represents the data has a slightly negative slope with temperature although a temperature dependence to the heat capacities is not resolvable within error. Therefore, temperature independent heat capacity values were determined by averaging the liquid data for each of the four samples (NAS-2, -8, -9, and –15). Both the temperature independent values and the temperature dependent fit equations for the C_P of the four samples are given in Table 3 and shown in Fig. 5a–f as a solid line/curve at temperatures above T_g.

In contrast to the results in this study, Richet and Bottinga (1984) observed a slight *increase* with temperature in

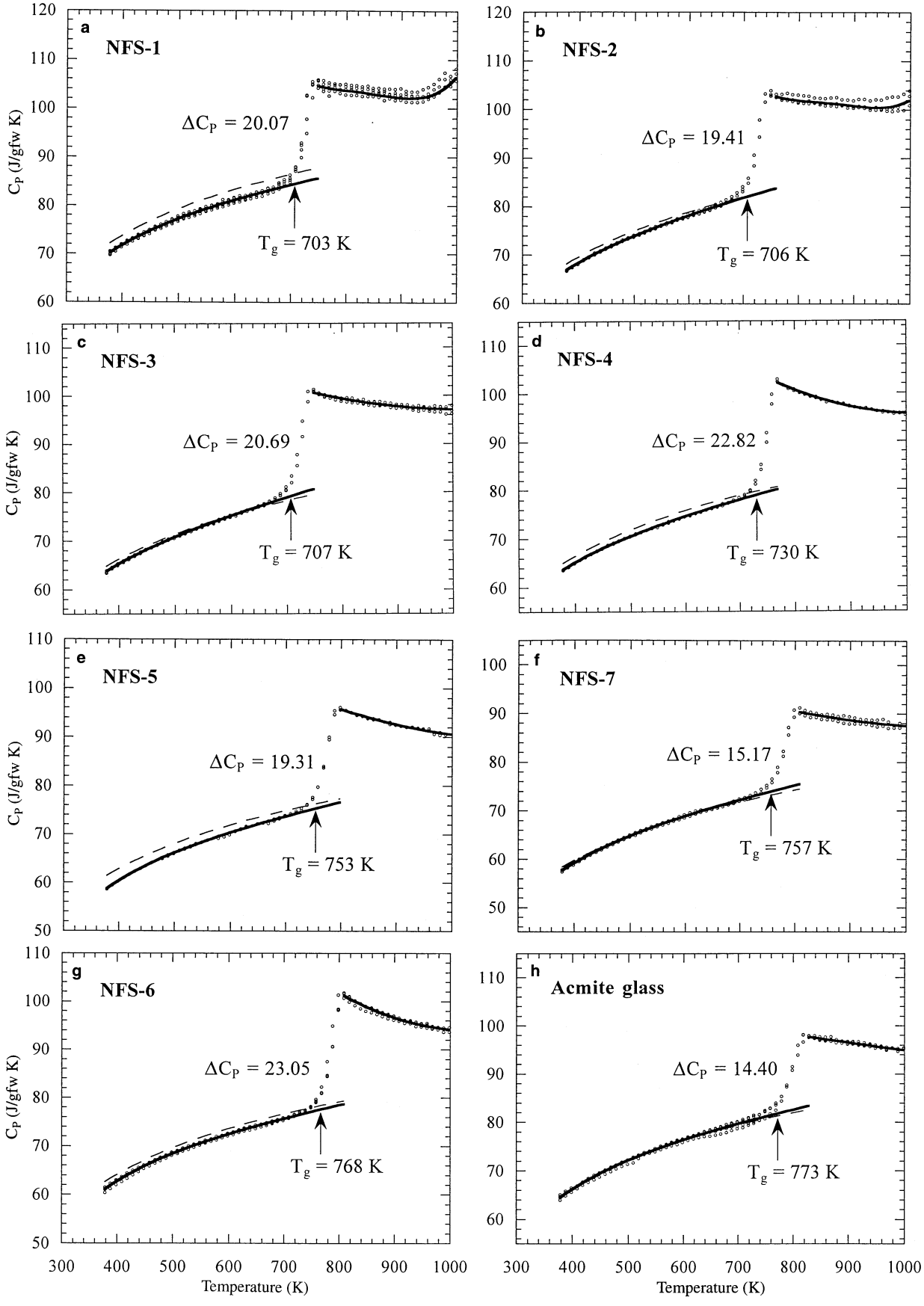
a
NFS-1
ΔCP = 20.07
Tg = 703 K
b
NFS-2
ΔCP = 19.41
Tg = 706 K
c
NFS-3
ΔCP = 20.69
Tg = 707 K
d
NFS-4
ΔCP = 22.82
Tg = 730 K
e
NFS-5
ΔCP = 19.31
Tg = 753 K
f
NFS-7
ΔCP = 15.17
Tg = 757 K
g
NFS-6
ΔCP = 23.05
Tg = 768 K
h
Acmite glass
ΔCP = 14.40
Tg = 773 K
CP (J/gfw K)
Temperature (K)

Fig. 6a–h

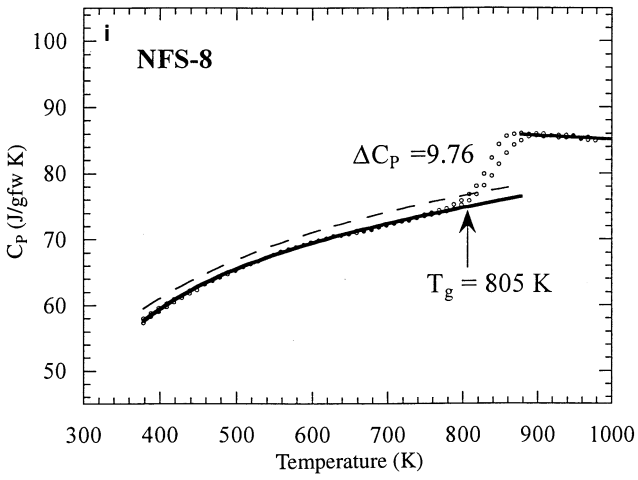

Fig. 6a–i Heat capacity data for nine compositions in the Na_2O-(FeO)-Fe_2O_3-SiO_2. Description of the details of each diagram are as in Fig. 4

the liquid C_P of sodium aluminosilicate glasses corresponding to albite ($NaAlSi_3O_8$), jadeite ($NaAlSi_2O_6$), and nepheline ($NaAlSiO_4$). However, these compositions have $Al_2O_3/Na_2O \geq 1$, unlike the sodium aluminosilicates in this study, which all have $Al_2O_3/Na_2O < 1$. In addition, the temperature range of the heat capacity measurements of Richet and Bottinga (1984) is much greater (albite: 1120–1791 K; jadeite: 1127–1810 K; nepheline: 1033–1834 K) and for all three mineral compositions, the temperature intervals over which C_P's were measured start at higher T's than the highest temperature (1003 K) of the C_P measurements in this study. Richet (1982) found that glasses in the Na_2O-Al_2O_3-SiO_2 system with $Al_2O_3/Na_2O \geq 1$ have liquid heat capacities that are temperature dependent and that for samples with $Al_2O_3/Na_2O < 1$, no temperature dependence can be resolved.

Sodium iron silicates

Two to four runs were performed for each of the sodium iron silicates, and the C_P data are plotted in Fig. 6a-i; the reproducibility is generally quite good. All of the supercooled liquid heat capacities of the sodium iron silicates show negative temperature dependent behavior. Data for the supercooled liquids of samples NFS-3, -4, -5, -6, and -7 were fitted to a second-order polynomial (Table 3; solid curve above T_g in Fig. 6c-g). The negative temperature dependence for these samples can be recovered upon cooling (reversal data for NFS-6 is shown in Fig. 3a) which indicates that the C_P data are derived from equilibrium measurements. The samples that show the greatest and least degree of temperature dependent behavior

Table 3 Coefficients for equations for supercooled liquid heat capacities: $C_P^{liq}=a+bT+cT^2+dT^3+eT^4$ (J/gfw K)

Sample	Avg. Liq. (1 σ)	a	$b\times10^3$	$c\times10^3$	$d\times10^6$	$e\times10^9$	T range (K)
NS-1	83.39 (0.96)	–	–	–	–	–	818–998
NS-2	86.12 (0.64)	–	–	–	–	–	788–998
NS-3	88.33 (0.84)	–	–	–	–	–	788–898
NS-4	90.35 (1.01)	–	–	–	–	–	778–878
NS-5	90.03 (1.30)	–	–	–	–	–	748–828
NS-6	91.24 (1.22)	–	–	–	–	–	738–798
NS-7	94.77 (0.80)	–	–	–	–	–	738–748
NAS-2	92.64 (0.34)	95.677	–3.2205	–	–	–	888–998
NAS-8	94.05 (0.51)	98.907	–5.4133	–	–	–	798–998
NAS-9	95.41 (0.58)	101.495	–6.5268	–	–	–	868–998
NAS-10	97.03 (0.25)	–	–	–	–	–	948–998
NAS-15	99.98 (0.74)	107.885	–8.4227	–	–	–	878–998
NAS-B	87.44 (0.45)	–	–	–	–	–	888-998
NFS-1	–	4299.870	–20220.3	36.547	–29.347	8.8271	748–998
NFS-2	–	4694.520	–21481.1	37.654	–29.305	8.5397	758–998
NFS-3	–	146.962	–97.877	0.047991	–	–	748–998
NFS-4	–	199.973	–203.413	0.099139	–	–	768–998
NFS-5	–	155.186	–113.604	0.048972	–	–	798–998
MFS-6	–	237.858	–276.411	0.132754	–	–	808–998
NFS-7	–	131.148	–79.004	0.035358	–	–	808–998
NFS-8	–	90.824	–5.6998	–	–	–	878–998
Acmite	–	110.942	–16.0413	–	–	–	828–998
NTS-1	–	107.419	–12.214	–	–	–	848–978
NTS-2	–	147.804	–42.811	–	–	–	888–978
NTS-3	–	107.586	–14.163	–	–	–	868–978
NTS-4	–	144.378	–41.634	–	–	–	808–978
NTS-5	–	184.754	–79.598	–	–	–	818–898
NTS-6	–	139.430	–39.823	–	–	–	928–978
LC-20	–	126.770	–27.344	–	–	–	868–978

Note: C_Ps calculated using these equations are reliable to two numbers following the decimal point

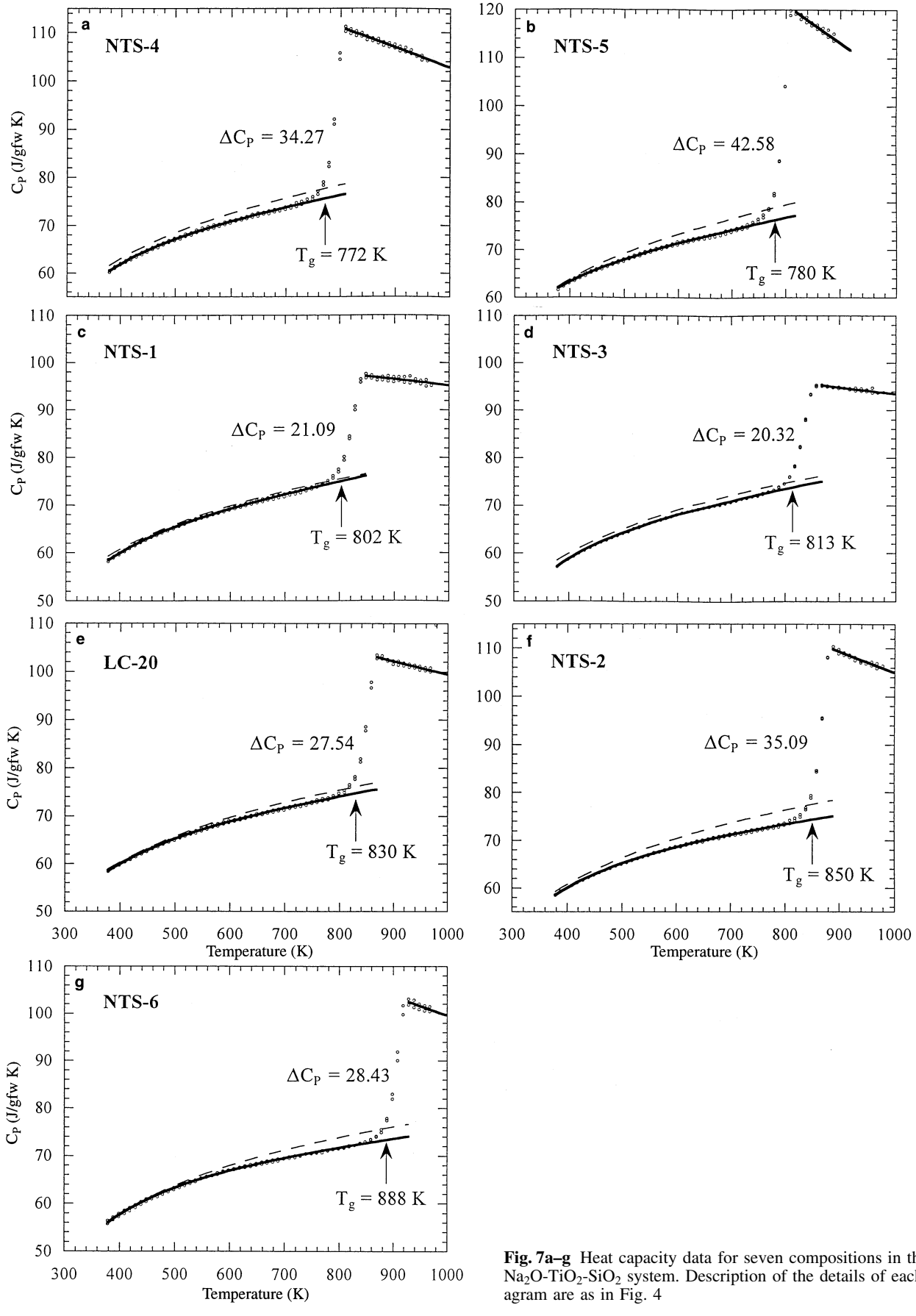

Fig. 7a–g Heat capacity data for seven compositions in the Na_2O-TiO_2-SiO_2 system. Description of the details of each diagram are as in Fig. 4

(NFS-6 and -4 vs. NFS-7) have the highest and lowest ferric iron contents, respectively (~10 versus ~2 mol%). The C_P data in the liquid region for NFS-8 and acmite glasses are linear with temperature as shown in Table 3 and by the solid curve above T_g in Fig. 6h, i. Both NFS-8 and acmite have at least as much as or more iron (~10 and ~15 mol% respectively) than NFS-6 and -4, but the negative temperature dependence of these two samples is less pronounced. Of all the iron-bearing samples investigated, NFS-1 has the highest concentrations of Fe_2O_3 (18 mol%) and Na_2O (39 mol%) and the lowest concentration of SiO_2 (43 mol%). The shape of the supercooled liquid curve for NFS-1 is unusual in that for approximately the first 200 degrees following T_g, there is a negative temperature dependence to the liquid heat capacity, but for about the last 100 degrees, the heat capacity increases rather markedly to produce a distinct and reproducible positive temperature dependence. The shape of the supercooled liquid curve for NFS-2 is similar to NFS-1 although less pronounced. For these two samples, the heating C_P data cannot be recovered during a DSC cooling run. The shapes of the heating and cooling curves for NFS-1, particularly in the supercooled liquid region are clearly different (Fig. 3b). The data for NFS-1 and NFS-2 liquids are reproduced best by a fourth order polynomial (Table 3, Fig. 6a, b). The polynomial fits are specific to these compositions and should only by applied within the temperature range of the calibration.

The measured heat capacities just above T_g of the sodium iron silicates in this study agree within 2% with those measured at much higher temperatures by Lange and Navrotsky (1992) (using a Setaram HT-1500 differential scanning calorimeter) for NFS-2, -4, -5, and -6. However, C_P data in this study for these samples at 998 K (the highest temperature of measurement) are significantly lower than the mean C_P data of Lange and Navrotsky (1992). Agreement between our data and that of Lange and Navrotsky (1992) for NFS-1 and -8 is generally poor, which in part reflects errors that originate not only from conductive heat loss, but also from radiative heat loss at the high temperatures of measurement in the Lange and Navrotsky (1992) study.

Sodium titanosilicates

Two separate DSC runs were performed on each of the sodium titanosilicate samples and are plotted in Fig. 7a–g; the reproducibility for all samples is within 1%. All of the samples show a marked negative temperature dependence to the liquid heat capacity. A simple linear fit was sufficient to accurately model the temperature-dependent liquid C_P data for each sample; coefficients of the fit equations are given in Table 3 and the fit is represented by the solid curve at temperatures above T_g in Fig. 7a–g. In general, the temperature dependence becomes more pronounced with increasing titanium content. Interlaboratory errors for the sodium titanosilicates can be evaluated by comparing C_P data on $Na_2O{\cdot}TiO_2{\cdot}2SiO_2$ from Richet and Bottinga (1985) and Lange and Navrotsky (1993) to those obtained in this study on the same composition (NTS-2). The relatively low-temperature liquid heat capacities for NTS-2 obtained in this study are within error of the heat capacity measurements of Richet and Bottinga (1985) obtained with high temperature drop calorimetry and Lange and Navrotsky (1993) obtained with a Setaram HT-1500 differential scanning calorimeter.

Discussion

Configurational versus vibrational contributions to heat capacity

The heat capacity of silicate glasses is derived primarily from interatomic vibrations that are insensitive to local structure above room temperature. Thus, values for the partial molar heat capacities of oxide components in glasses are within a few percent of those in corresponding pure crystalline solids (Richet and Bottinga 1986). With continuous heating of a glass, the number of accessible vibrational modes and the heat capacity both increase. The abrupt increase in C_P at T_g reflects the additional energy needed to activate translational and rotational degrees of freedom. The attainment of these configurational degrees of freedom may involve changes in bond lengths and angles, nearest and next-nearest neighbor distances, and coordination numbers (Richet and Bottinga 1995). The magnitude of the jump in C_P at T_g is related to the availability of new configurations above T_g which, in turn, is related to the short- and intermediate-range structure of the liquids.

The configurational heat capacity for the 29 samples was determined by subtracting the heat capacity of the glass (using the individual fitted glass curve) at the same temperature as the first usable data point for the heat capacity of the supercooled liquid. These temperatures are given in Table 3 as the lowest temperature in the range over which the equations were fitted to the data for the liquid. For the sodium silicates and the sodium aluminosilicates, values for the liquids are the constants given in Table 3. For the sodium titanosilicates and the sodium iron silicates, the value for the liquid used in the determination of the configurational heat capacity was the average of the set of data points at the specified temperature.

For the sodium silicate glasses, the configurational heat capacities at T_g increase linearly with Na_2O content for compositions with less than ~35 mol % Na_2O and the $C_P^{conf}(T_g)$ for all of the sodium silicate samples remains below an apparent upper limit of about 16% (Fig. 8). Similarly, for the six sodium aluminosilicates, the configurational heat capacities increase with Na_2O content and appear to be independent of Al_2O_3 content, but again, the configurational heat capacities (at T_g) do not exceed a threshold of about 16%. This apparent upper limit of the configurational heat capacities in both the sodium silicate and sodium aluminosilicate systems is a possible indication that the number of new configurations

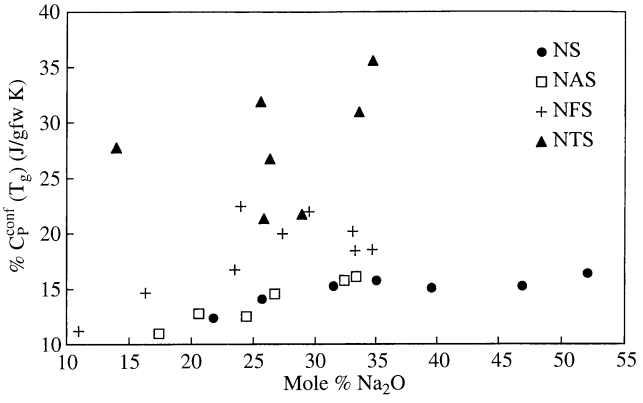

Fig. 8 Percent C_P^{conf} at $\sim T_g$ versus mole% Na_2O for Na_2O-SiO_2 (NS), Na_2O-Al_2O_3-SiO_2 (NAS), Na_2O-(FeO)-Fe_2O_3-SiO_2 (NFS), and Na_2O-TiO_2-SiO_2 (NTS) systems

which can be accessed in these systems reaches saturation. In contrast, the configurational heat capacities in the iron- and titanium-bearing systems, in general, significantly exceed the values of those in the sodium silicate and sodium aluminosilicate systems. It follows that the presence of Fe^{3+} and Ti^{4+} may allow 'extra' configurational rearrangements to be accessed in the sodium iron silicate and sodium titanosilicate melts.

For both the sodium silicate and sodium aluminosilicate systems, the heat capacity of the supercooled liquids is independent of temperature within the resolution of the data. For samples in the sodium iron silicate and sodium titanosilicate systems, no correlation between the Na_2O contents and the configurational heat capacities is apparent (Fig. 8). Moreover, the configurational heat capacity of the iron- and titanium-bearing systems appears strongly dependent on the Fe_2O_3 and TiO_2 contents. The configurational heat capacities at T_g in these systems are in many cases significantly greater than those in the sodium silicate and sodium aluminosilicate systems for samples with roughly similar Na_2O concentrations.

The observation that the configurational heat capacities of sodium aluminosilicates increase linearly with Na_2O concentrations and are independent of Al_2O_3 content, whereas those of the iron- and titanium-bearing silicates do not, and instead depend on Ti^{4+} and Fe^{3+}, is compelling. Since Al^{3+}, Fe^{3+}, and Ti^{4+} are all network forming cations, it might be expected that the three systems would show similar behavior in the liquid region. In a study on the thermal expansivity of sodium aluminosilicate melts, Lange (1996) found that within error only the Na_2O component contributes to the configurational thermal expansivity of the melts. This is consistent with the observation that the configurational heat capacities of the sodium aluminosilicates in this study are independent of Al_2O_3 content and linearly correlated with Na_2O content. Furthermore, the thermal expansivities of the sodium aluminosilicates are temperature independent over a temperature interval of greater than 1000 degrees (Lange 1996). The apparent correlation between the configurational heat capacities and the thermal expansivities of the sodium aluminosilicate melts leads to speculations regarding those properties in the iron- and titanium-bearing melts. It is expected that the iron- and titanium-bearing melts would have temperature dependent thermal expansivities to which the Fe_2O_3 and TiO_2 components contribute.

Compositional model of liquid heat capacities

Using high temperature drop calorimetric methods, Richet et al. (1984) measured the relative enthalpies of four sodium silicate liquids over a temperature range of 900–1800 K. They found that the derived heat capacities of these liquids displayed no observable temperature dependence and could be modelled as a linear function of composition according to the equation:

$$C_P^{liq} = \sum X_i C_{P,i}^{liq} \tag{2}$$

where C_P^{liq} is the heat capacity of the liquid, X_i is the mole fraction of component i, and $C_{P,i}^{liq}$ is the partial molar heat capacity of component i in the liquid. The partial molar heat capacity values for Na_2O and SiO_2 determined by Richet et al. (1984) are 100.6 and 81.37 J/mole K, respectively. Using these partial molar values, the resulting model heat capacities corresponding to the compositions of the seven samples in this study are plotted in Fig. 4a–g and listed in Table 3. The agreement is ≤2.5% (NS-2 being the best, and NS-7 being the worst). By fitting data for the Na_2O-SiO_2 liquids in this study to Eq. (2), $C_{P,i}$ values (±1σ) of 110.7±0.5 and 77.1±0.2 J/mol K for Na_2O and SiO_2, respectively, were obtained. For the seven samples in the Na_2O-SiO_2 system, the compositional dependence of the heat capacity of the liquid can be modelled with residuals ≤1.7%.

The C_P data for the sodium aluminosilicates were also fit to Eq. (2) to obtain $C_{P,i}$ values (±1σ) of 120.0±0.5, 145.9±1.0, and 74.5±0.2 J/mol K for Na_2O, Al_2O_3, and SiO_2 systems, respectively. When data for the sodium silicate liquids and the sodium aluminosilicate liquids were combined and fitted to Eq. (2), derived values for $C_{P,i}$ of 112.4±0.4, 153.2±0.8, and 76.4±0.2 J/mol K for Na_2O, Al_2O_3, and SiO_2, respectively, were obtained. Using these values, the compositional dependence of the heat capacities of the liquids in both the Na_2O-SiO_2 and the Na_2O-Al_2O_3-SiO_2 systems was modelled with residuals ≤2.1%. Although this error is within experimental error, liquid C_P residuals of 2% (versus glass C_P residuals of 1%) may reflect the likely possibility that the configurational contributions to the C_P of the supercooled liquid (versus the vibrational contribution) are not additive with respect to composition (X_i). In this study, it is apparent that for sodium silicate liquids with >35 mole % Na_2O, sodium iron silicates, and sodium titanosilicates, the C_P^{conf} is not additive with respect to composition. A reasonable inference may be that the configurational C_P depends on local structure unlike the vibrational C_P.

Sub-microscopic domains in the Na_2O-TiO_2-SiO_2 system

For five of the seven sodium titanosilicates in this study, the jump in heat capacity at T_g is significantly greater than for any of the samples in the other three silicate systems investigated. The two NTS samples with the lowest TiO_2 contents have C_P^{conf} values that are similar in magnitude to six of the sodium iron silicate samples. In addition, the liquid heat capacities of all of the sodium titanosilicates decrease with temperature. In general, the higher the TiO_2 content, the stronger the temperature dependence. Both Richet and Bottinga (1985) and Lange and Navrotsky (1993) reported heat capacity measurements on a $Na_2TiSi_2O_7$ liquid, which is the same as that of NTS-2 in this study. All three sets of data are within error of one another. Following the suggestion of Lange and Navrotsky (1993) that the anomalously high configurational heat capacity at the glass transition and its subsequent decrease with temperature in alkali titanosilicate melts may be related to coordination changes involving Ti^{4+}, a number of studies were undertaken to elucidate the structure of these melts. Mysen and Neuville (1995) used micro-Raman spectroscopy to examine the effect of temperature and TiO_2 content on the structure of $Na_2Si_2O_5$-$Na_2Ti_2O_5$ melts and glasses. They observed that the NBO/T of the samples increased across the glass transition interval and that this was followed by a decrease as the temperature was increased further. They suggested that the unusual C_P behavior documented by Richet and Bottinga (1985) and Lange and Navrotsky (1993) could be explained by this temperature dependent NBO/T variation.

Farges et al. (1996a, b) used *in situ* Ti K-edge XAFS spectroscopy to determine the local structural environment of Ti in some Na, K, and Ca-titanosilicate glasses/melts between 293 and 1650 K. In the Na- and K-titanosilicate samples, which demonstrate a strong negative temperature dependence to their C_P above T_g, Farges et al. (1996a) found no clear evidence for any significant change in the average nearest neighbor coordination of Ti^{4+} in these glasses and melts with temperature. They did observe, however, significant changes in the medium-range environment around Ti^{4+} above T_g. These changes involved increases in Ti–Si and Ti–M distances (M=Na, K, Ca).

Farges et al. (1996c) found that $^{[5]}$Ti (five-coordinated Ti) is the dominant Ti species in the glasses with >16 wt % TiO_2. In addition, each of the $^{[5]}$Ti is in a distorted square pyramid, the base of which is formed by four long Ti–O bonds and the apex of which is defined by one short Ti=O (titanyl) bond. Using a combination of EXAFS, Ti X-ray absorption near edge structure (XANES) spectra, and experimental Ti-pre-edge data with bond-valence constraints, Farges et al. (1996c) developed a model describing the longer range order in titanosilicate glasses which contain the $(^{[5]}Ti{=}O)O_4$ square pyramids. They suggested that Ti in the $(^{[5]}Ti{=}O)O_4$ form acts as both a network former and a network modifier, with the network former role dominating. The oxygen in the short Ti=O bonds is shared only with alkali cations and the four oxygens forming the base of the $(^{[5]}Ti{=}O)O_4$ pyramid are shared with Si (and/or Ti) and at least two alkali cations. The longer range order proposed by Farges et al. (1996b), which results from the short range configuration of $^{[5]}$Ti, is characterized by two regions in the glass, a relatively less polymerized region dominated by network modifiers (alkalis) with adjacent titanyl units and a relatively more polymerized region dominated by network formers and connected to the Ti–O bonds. The regions rich in network modifiers are the percolation domains. Farges et al. (1996b) suggested that a possible cause of the anomalously high configurational heat capacity at T_g observed in alkali titanosilicates involves an increase in the number of second-neighbor (Na and K) configurations around Ti in the percolation domains. Furthermore, at temperatures exceeding T_g, Farges et al. (1996c) speculated that it is the breakdown of the percolation domains and the subsequent homogenization of the melt which results in the observed decrease with temperature of the configurational C_P of the alkali titanosilicate melts.

Could percolation domains be present in the Na_2O-(FeO)-Fe_2O_3-SiO_2 liquids?

A similar scenario involving the attainment of a greater number of configurations for the low field strength cations in the percolation domains at glass transition temperatures and the subsequent breakdown of these domains at temperatures exceeding T_g may occur in the sodium iron silicates. The configurational heat capacities of the sodium iron silicate liquids are, on average, greater than those of the sodium silicate and sodium aluminosilicate liquids. In addition, for the majority of the samples, the decrease in the configurational heat capacity with temperature is qualitatively similar to that seen in alkali titanosilicate melts. The combination of these characteristics is suggestive of some type of melt restructuring.

Spectroscopic data are necessary to elucidate the type of structural rearrangements in the melt phase to which the anomalous macroscopic thermodynamic properties can be attributed. An important aspect of the atomic structure in silicate glasses and melts is the coordination environment of ferric iron, which is a subject of considerable controversy. Hannoyer et al. (1992) provided an extensive list of the sites for Fe^{3+} in alkali silicate and soda lime silicate glasses that have been reported in the literature. These coordination environments have been determined using a variety of physical techniques including optical, electron paramagnetic resonance and Mössbauer spectroscopies, XANES spectra and extended XAFS spectroscopy. The preponderance of data indicates that ferric iron is most commonly in tetrahedral coordination in alkali and soda lime silicate glasses (Bamford 1960; Steele and Douglas 1965; Kurkjian and Sigety 1968; Hirao et al. 1979; Fox et al. 1982; Greaves et al. 1984; Brown et al. 1986; Wang et al. 1993, 1995). However, some studies have concluded that both tetrahedral and octahedral Fe^{3+}

are present in alkali silicate and soda lime silicate glasses (Levy et al. 1976; de Grave 1980; Fenstermacher 1980; Calas and Petiau 1983; Wang and Chen 1987; Hannoyer et al. 1992). Hannoyer et al. (1992) presented spectroscopic evidence which indicates that the proportion of octahedral Fe^{3+} decreases with increasing amounts of Fe^{3+} in glasses containing the same total iron. This is in accord with studies by Baiocchi et al. (1982) and Mysen (1987) and is consistent with EXAFS measurements conducted by Park and Chen (1982), on the basis of which it was concluded that Fe^{3+} is in octahedral coordination in dilute concentrations in sodium disilicate glasses.

Because of the trivalent nature of both Al and Fe ions in the Na_2O-M_2O_3-SiO_2 systems and their role as network formers, it is useful to compare some of the available spectroscopic data for the two cations. Unlike Fe^{3+}, much of the structural data for Al^{3+} is derived from NMR studies (Stebbins 1995); the paramagnetic properties of Fe^{3+} preclude the application of NMR spectroscopy to iron-bearing silicate glasses/melts. Similar to what has been concluded for Fe^{3+}, spectroscopic data for Al^{3+} indicate that the coordination is commonly tetrahedral at one bar (Taylor and Brown 1979a,b; Taylor et al. 1980; Engelhardt and Michel 1987; Oestrike et al. 1987). However, it has also been found to exist in both five- and six-fold coordination in peraluminous silicate glasses at ambient pressure (Risbud et al. 1987; Bunker et al. 1991; Sato et al. 1991a, b; Poe et al. 1992).

Although both ferric iron and aluminum are trivalent network formers, they differ significantly in their electronegativity and chemical affinity. In addition, the temperature dependence of the heat capacities of the supercooled liquids in the Na_2O-Al_2O_3-SiO_2 system is much less pronounced (and in some cases nonexistent; NAS-10, NAS-B) than that in the Na_2O-(FeO)-Fe_2O_3-SiO_2 system. As mentioned previously, the negative temperature dependence of the heat capacities of the sodium iron silicate liquids is qualitatively more similar to that of the sodium titanosilicates. Therefore, an examination of the coordination environment of Ti^{4+} may be more relevant to the discussion of the structural role of Fe^{3+} .

Farges et al. (1996a) pointed out that because the most common coordination environments for Ti^{4+} in crystalline oxides are tetrahedral and octahedral, most studies investigating the structural state of Ti^{4+} in oxide glasses have focused on TiO_4 and TiO_6 units. However, $^{[5]}Ti^{4+}$ is known to occur in crystalline silicates such as fresnoite ($Ba_2{}^{[5]}TiSi_2O_8$; Markgraf et al. 1985) and $Na_2(^{[5]}TiO)SiO_4$ (Egorov et al. 1978; Nyman et al. 1978) and oxides such as $K_2{}^{[5]}Ti_2O_5$ (Andersson and Wadsley 1974). Using materials such as these as well as $^{[4]}Ti^{4+}$- and $^{[6]}Ti^{4+}$-bearing silicates as model compounds in a series of XAFS measurements on a variety of alkali titanosilicate glasses and liquids, Farges et al. (1996b, c) found that a significant portion of the Ti^{4+} in the glasses and liquids was present in pentacoordinate complexes.

Like Ti^{4+}, ferric iron has also been found in five-fold coordination in a few silicate minerals. The presence of $^{[5]}Fe^{3+}$ has been reported in vesuvianite at room temperature (Olesch 1979), andalusite at ambient temperature and at 77 K (Abs-Wurmbach et al. 1981), and orthoericssonite from 78–547 K (Halenius 1995). Although a body of XAFS data analogous to that for the alkali titanosilicates is not yet available for alkali iron silicates, Mössbauer data indicate that Fe^{3+} may be present in pentacoordinated sites in some silicate glasses and melts. Bychkov et al. (1993) fitted the spectrum of acmite glass to several doublets without constraints and derived an estimate for the isomeric shift which indicated an effective value of five for the coordination number of the glass. For the most part however, because pentacoordinated cations (e. g., $^{[5]}Ti^{4+}$ and $^{[5]}Fe^{3+}$) in silicate mineral structures are rare, spectroscopic data on cations at such sites are scarce as well.

Bychkov et al. (1992) noted that the lack of long range order in glasses increases the probability that the network-forming and network-modifying cations will have a range of coordination states. In addition, the cation-ligand bond lengths in the polyhedra may vary much more than in crystals. In light of this and the available structural information on Al^{3+}, Ti^{4+}, and Fe^{3+}, the possibility that all three coordination states ($^{[4]}Fe^{3+}$, $^{[5]}Fe^{3+}$, and $^{[6]}Fe^{3+}$) coexist in silicate glasses and liquids cannot be dismissed. Moreover, like $^{[5]}Ti^{4+}$, $^{[5]}Fe^{3+}$ may be present in amorphous silicates as a distorted square pyramid, as described for orthoericssonite (Matsubara 1980). If $^{[5]}Fe^{3+}$ is present in the sodium silicate melts of this study, and an analogy is drawn between the Ti and Fe-bearing melts, the existence of submicroscopic domains (relatively polymerized and depolymerized regions in the melt) may contribute to the observed anomalies in the configurational heat capacities of the sodium iron silicates. Recent Raman studies on glasses and melts in the sodium iron silicate system supports this view (Wang et al. 1993, 1995).

Q^n speciation changes in Na_2O-(FeO)-Fe_2O_3-SiO_2 melts: are they related to the breakdown of a domain structure?

In a combined *in situ* Raman and Mössbauer spectroscopic study between 293 and 1044 K, Wang et al. (1993, 1995) found no evidence for a change in the coordination of Fe^{3+} in two Na_2O-FeO-Fe_2O_3-SiO_2 liquids (similar to NFS-4 and NFS-6; both of which demonstrate a marked negative C_P temperature dependence). Furthermore, through an analysis of their high temperature Raman data, Wang et al. (1993, 1995) observed that the contribution to the high-frequency Raman envelope related to the Q^3 stretching band increases with temperature. This increase is most pronounced in a 200 degree interval near the glass transition. They suggested two possible interpretations, which are not mutually exclusive, and which could account for the anomalous increase in the intensities of the Raman bands associated with Q^3 species relative to those of the Q^4 species. Either a selective change in the Raman scattering cross sections with temperature or a net increase in the proportion of Q^3 species could explain their spectroscopic observations.

If the data of Wang et al. (1993, 1995) are explained by a net increase in the proportion of Q^n species with temperature, some sort of disproportionation reaction may be occurring in the iron-bearing melts. At temperatures greater than T_g, the distribution of Q^n species [where Q denotes quaternary (four bonds) and n is the number of bridging oxygens (BO) per tetrahedrally coordinated cation] can be described by the model equation:

$$2Q^n = Q^{n+1} + Q^{n-1} \quad (4 > n > 0). \tag{3}$$

For the melts in this study, which have NBO/T (where NBO refers to non-bridging oxygen and T refers to the number of tetrahedrally coordinated cations) values between 0.03 and 0.68, assuming tetrahedrally coordinated Fe^{3+}, only Q^2, Q^3 and Q^4 species should predominate (e.g., Murdoch et al. 1985; Mysen and Frantz 1992). The distribution of these species in a melt is shown by the equilibrium reaction:

$$2Q^3 = Q^4 + Q^2. \tag{4}$$

As an example, all of the Si tetrahedra are Q^3 species in the $Na_2Si_2O_5$ crystal. In contrast, *in situ* NMR (nuclear magnetic resonance) spectroscopic studies by Brandriss and Stebbins (1988) and Stebbins (1987, 1988) showed that all three Q species (with Q^3 species dominating) are present in $Na_2Si_2O_5$ glass and liquid. With increasing temperature reaction Eq. (4) proceeds to the right, consistent with the concept that the liquid becomes more disordered and its entropy increases with temperature (Stebbins 1987, 1988; Brandriss and Stebbins 1988; Mysen and Frantz 1992).

On the other hand, the spectroscopic analyses by Wang et al. (1993, 1995) on the two sodium iron silicate melts which are similar in composition to NFS-4 and NFS-6 in this study, indicate that there may be an increase in the proportion of Q^3 species with temperature. If Eq. (4) is applicable, then the Q^n-disproportionation reaction direction is to the left with increasing temperature above T_g (to 1044 K, the high-T limit of their Raman spectroscopic experiments). This leftward shift of the equilibrium direction for the reaction is opposite to that observed in sodium silicate melts (Brandriss and Stebbins 1988).

At first glance, the possibility of a displacement of equilibrium (4) to the reactant side appears to suggest that the Na_2O-(FeO)-Fe_2O_3-SiO_2 liquids are becoming more ordered with increasing temperature immediately above T_g. However, if the Raman spectroscopic data of Wang et al. (1993, 1995) are considered in the context of submicroscopic domains in the liquid, a different interpretation may be formulated. If the Na_2O-(FeO)-Fe_2O_3-SiO_2 liquids are similar to the Na-and K-bearing titanosilicate melts investigated by Farges et al. (1996a, b), there may be two distinct domains in the sodium iron silicate melts at low temperatures immediately above T_g: one relatively polymerized (with a higher abundance of Q^4 species), and another relatively depolymerized (with a higher abundance of Q^2 species). If these submicroscopic domains break down with increasing temperature (as proposed for the alkali titanosilicate melts), then the abundance of Q^3 species should increase relative to Q^2 and Q^4 species, as observed (Wang et al. 1993, 1995). The breakdown of two distinct domains in the melt to a more homogeneous melt structure is consistent with the concept of increasing disorder and entropy in the melt with increasing temperature.

Brandriss and Stebbins (1988) determined that the effect of Q-speciation changes on the configurational heat capacity in silicate melts is negligible. It should be clarified that it is not the Q-speciation changes in the sodium iron silicate melts that are being proposed as the cause of the anomalous configurational heat capacities. Rather, it is the possibility that the intermediate range order in the iron bearing melts is characterized by a domain structure which breaks down with temperature, thereby resulting in the anomalous temperature dependent C_{PS}.

Farges et al. (1996b) argued that the percolation domains observed in the alkali titanosilicate melts by Ti K-edge XAFS spectroscopy were related to the dual structural role of five-coordinated Ti (the dominant Ti species in those glasses and melts). They showed that $^{[5]}$Ti occurs at the interface of percolation domains, with the titanyl oxygens of the square-pyramidal units oriented toward the network-modifier enriched regions (with a relative abundance of Q^2 species) and the bridging oxygens associated with the four longer Ti–O bonds oriented toward the network-former enriched regions (with a relative abundance of Q^4 species). The question that arises is whether Fe^{3+} in a sodium silicate melt plays a similar role as the square-pyramidal units of $^{[5]}$Ti. Bond valence models are not consistent with the prediction of a five-coordinated Fe^{3+} unit similar to that of the titanyl unit (Brown et al. 1995). However, the available spectroscopic data do not rule out the possible existence of $^{[5]}Fe^{3+}$. The domain structure proposed for alkali titanosilicate melts is not predicated on the existence of the titanyl units. Therefore, it follows that submicroscopic domains in the sodium iron silicates may exist even if $^{[5]}Fe^{3+}$ does not.

The negative temperature dependence of the liquid heat capacity in the sodium-iron-silicates may have its origin in the breakdown of microscopic domains involving relatively polymerized (dominated by Q^4 species) and non-polymerized (dominated by Q^2 species) regions of the melt. The dynamic changes in melt structure that occur in the Na_2O-(FeO)-Fe_2O_3-SiO_2 melts with temperature, whether they are related to the possible occurrence of $^{[5]}Fe^{3+}$ and/or a breakdown in domain structure, have a significant effect on the bulk thermodynamic properties and in turn the transport properties of the melts. Since Fe_2O_3 is often a significant component in natural magmatic liquids, understanding its behavior in relatively simple synthetic liquids at relevant magmatic temperatures is a first step to determining its role in natural systems.

Acknowledgements This study was supported by NSF grants EAR-9405768 and 9304162. We thank Ian Carmichael for performing wet chemical analyses on the samples and we thank F. Farges and an anonymous referee for their insightful reviews and D. Kohlstedt for editorial handling.

References

Abs-Wurmbach I, Langer K, Seifert F, Tillmanns E (1981) The crystal chemistry of (Mn^{3+},Fe^{3+})-substituted andalusites (viridines and kanonaite),$(Al_{1-x-y}Mn^{3+}_xFe^{3+}_y)_3(O|SiO_4)$: crystal structure refinements, Mössbauer and polarized optical absorption spectra. Z Kristalloqr 155:81–113

Andersson S, Wadsley AD (1974) The crystal structure of $K_2Ti_2O_5$. Acta Chem Scand 15:663–669

Baiocchi E, Bettinelli M, Montenero A, di Sipio L (1982) Spectroscopic behavior of iron(III) in silicate glass. J Am Ceram Soc 65:39–40

Bamford CR (1960) A study of the magnetic properties of iron in relation to its colouring action in glass. I. Iron in sodium borate glasses melted under oxidizing conditions. Phys Chem Glasses 1:159–164

Bosenick A, Geiger CA, Cemic L (1996) Heat capacity measurements of synthetic pyrope-grossular garnets between 320 and 1000 K by differential scanning calorimetry. Geochim Cosmochim Acta 60:3215–3227

Brandriss ME, Stebbins JF (1988) Effects of temperature on the structures of silicate liquids: Si-29 NMR results. Geochim Cosmochim Acta 52:2659–2669

Brown GE Jr, Farges F, Calas G (1995) X-ray scattering and x-ray spectroscopy studies of silicate melts. In: Stebbins JF, McMillan PF, Dingwell DB (eds) Structure, dynamics and properties of silicate melts. Mineralogical Society of America, Washington DC, pp 318–410

Brown GE Jr, Waychunas GA, Ponader CW, Jackson WE, McKeown DA (1986) EXAFS and NEXAFS studies of cation environments in oxide glasses. J Phys Colloq (Paris) 47:661–668

Bunker BC, Kirkpatrick RJ, Brow RK, Turner GL, Nelson C (1991) Local structure of alkaline-earth boroaluminate crystals and glasses: II, ^{11}B and ^{27}Al MAS NMR spectroscopy of alkaline-earth boroaluminate glasses. J Am Ceram Soc 74:1430–1438

Bychkov AM, Polosin AV, Borisov AA (1992) A Mössbauer study on the effects of melt temperature on structural state of Fe ions. Geochem Int 29:141–148

Bychkov AM, Borisov AA, Khramov DA, Urusov VS (1993) Change in the immediate environment of Fe atoms during the melting of minerals (Review). Geochem Int 30:1–25

Calas G, Petiau J (1983) Coordination of iron in oxide glasses through high-resolution K-edge spectra: information from the pre-edge. Solid State Commun 48:625–629

Ditmars DA, Douglas TB (1971) Measurements of the relative enthalpy of pure α-Al_2O_3 (NBS Heat capacity and enthalpy reference material No. 720) from 273 to 1173 K. J Res 75 A:401–420

de Grave E, Chambaere D, van Iseghem P, de Batist R (1980) Mössbauer spectroscopic study of some complex M_2O-Mo-M_2O_3-SiO_2 glasses. J Phys Colloq (Paris) 41:269–270

Egorov T, Ye K, Simonov MA, Belov NV (1978) A revised crystal structure for synthetic sodium titanosilicate. Sov Phys Dokl 23: 289–290

Engelhardt G, Michel D (1987) High-resolution solid-state NMR of silicates and zeolites. John Wiley and Sons, New York

Farges F, Brown GE, Rehr JR (1996a) Coordination chemistry of Ti(IV) in silicate glasses and melts: I. XAFS study of titanium coordination in oxide model compounds. Geochim Cosmochim Acta 60:3023–3038

Farges F, Brown GE, Navrotsky A, Gan H, Rehr JR (1996b) Coordination chemistry of Ti(IV) in silicate glasses and melts: II. Glasses at ambient temperature and pressure. Geochim Cosmochim Acta 60:3039–3053

Farges F, Brown GE, Navrotsky A, Gan H, Rehr JR (1996c) Coordination chemistry of Ti(IV) in silicate glasses and melts: III. Glasses and melts from ambient to high temperatures. Geochim Cosmochim Acta 60:3055–3065

Fenstermacher JE (1980) Optical absorption due to tetrahedral and octahedral ferric iron in silicate glasses. Non-Cryst Solids 38–39:239–244

Fox KE, Furukawa T, White WB (1982) Transition metal ions in silicate melts. II. Iron in sodium silicate glasses. Phys Chem Glasses 23:169–178

Greaves GN , Binsted N, Henderson CMB (1984) The environments of modifiers in oxide glasses. In: Hodgson KO, Hedman B, Penner-Hahn JE (eds) EXAFS and Near Edge Structure III, Springer-Verlag, Berlin, 297–301

Halenius U (1995) A Mössbauer study of pentacoordinated ferric iron in orthoericssonite. Mineral J 17:363–371

Hannoyer B, Lenglet M, Dürr J, Cortes R (1992) Spectroscopic evidence of octahedral iron (III) in soda-lime silicate glasses. J Non-Cryst Solids 151:209–216

Hirao K, Soga N, Kunugi M (1979) Mössbauer and ESR analysis of the distribution of Fe^{3+} in leucite-type iron silicate glasses and crystals. J Am Ceram Soc 62:109–110

Johnson T, Carmichael ISE (1987) The partial molar volume of TiO_2 in multicomponent silicate melts. Geol Soc Am Abstr Prog 19:719

Knoche R, Dingwell DB, Seifert FA, Webb SL (1994) Non-linear properties of supercooled liquids in the system Na_2O-SiO_2. Chem Geol 116:1–16

Kurkjian CR, Sigety EA (1968) Coordination of the ferric ion in glass. Phys Chem Glasses 9:73–83

Lange RA (1996) Temperature independent thermal expansivities of sodium aluminosilicate melts between 713 and 1835 K. Geochim Cosmochim Acta 60:4989–4996

Lange RA, Carmichael ISE (1987) Densities of Na_2O-K_2O-CaO-MgO-FeO-Fe_2O_3-Al_2O_3-TiO_2-SiO_2 liquids: new measurements and derived partial molar properties. Geochim Cosmochim Acta 51:2931–2946

Lange RA, Carmichael ISE (1989) Ferric-ferrous equilibria in Na_2O-FeO-Fe_2O_3-SiO_2 melts: effects of analytical techniques on derived partial molar volumes. Geochim Cosmochim Acta 53:2195–2204

Lange RA, Navrotsky A (1992) Heat capacities of Fe_2O_3-bearing silicate liquids. Contrib Mineral Petrol 110:311–320

Lange RA, Navrotsky A (1993) Heat capacities of TiO_2-bearing silicate liquids: evidence for anomalous changes in configurational entropy with temperature. Geochim Cosmochim Acta 57:3001–3011

Levy RA, Lupis CHP, Flinn PA (1976) Mössbauer analysis of the valence and coordination of iron cations in SiO_2-Na_2O-CaO glasses. Phys Chem Glasses 17: 94–103

Markgraf SA, Halliyal A, Bhalla AS, Newnham RE (1985) X-ray structure refinement and pyroelectric investigation of fresnoite, $Ba_2TiSi_2O_8$. Ferroelectrics 62:17–26

Matsubara S (1980) The crystal structure of orthoericssonite. Mineralogical J 10:107–121

Mraw SC (1988) Differential scanning calorimetry. In: Ho CY (ed) Specific Heat of Solids, CINDAS Data Series on Material Properties: Vol I-2. Hemisphere Publishing Corporation, New York, pp 395–437

Murdoch JB, Stebbins JF, Carmichael ISE (1985) High-resolution ^{29}Si NMR study of silicate and aluminosilicate glasses: the effect of network-modifying cations. Am Mineral 70:332–343

Mysen BO (1987) Redox equilibria and coordination of Fe^{2+} and Fe^{3+} in silicate glasses from ^{57}Fe Mössbauer spectroscopy. J. Non-Cryst Solids 95–96:247–254

Mysen BO, Frantz JD (1992) Raman spectroscopy of silicate melts at magmatic temperatures: Na_2O-SiO_2, K_2O-SiO_2 and Li_2O-SiO_2, binary compositions in the temperature range 25–1475°C. Chem Geol 96:321–332

Mysen BO, Neuville D (1995) Effect of temperature and TiO_2 content on the structure of $Na_2Si_2O_5$-$Na_2Ti_2O_5$ melts and glasses. Geochim Cosmochim Acta 59:325–342

Nyman H, O'Keefe M, Bovin JO (1978) Sodium titanium silicate, Na_2TiSiO_5. Acta Crystallogr B34:905–906

Oestrike R, Yang W-H, Kirkpatrick RJ, Hervig RL, Navrotsky A, Montez B (1987) High-resolution ^{23}Na, ^{27}Al, and ^{29}Si NMR spectroscopy of framework aluminosilicate glasses. Geochim Cosmochim Acta 51:2199–2210

Olesch M (1979) Natürliche und synthetische Fe-haltige Vesuviane. Fortschr Mineral 57:114–115

Park JW, Chen H (1982) The coordination of Fe^{3+} in sodium disilicate glass. Phys Chem Glasses 23:107–108

Poe BT, McMillan PF, Angell CA, Sato RK (1992) Al and Si coordination in SiO_2-Al_2O_3 glasses and liquids: study by NMR and IR spectroscopy and MD simulations. Chem Geol 96:333–349

Richet P (1982) Propriétés thermodynamiques des silicates fondus. Thèse Université Paris 7:322 pp

Richet P (1987) Heat capacity of silicate glasses. Chem Geol 62:111–124

Richet P, Bottinga Y (1984) Glass transitions and thermodynamic properties of amorphous SiO_2, $NaAlSi_nO_{2n+2}$ and $KAlSi_3O_8$. Geochim Cosmochim Acta 48:453–470

Richet P, Bottinga Y (1985) Heat capacity of aluminum-free liquid silicates. Geochim Cosmochim Acta 49:471–486

Richet P, Bottinga Y (1986) Thermochemical properties of silicate glasses and liquids: a review. Rev Geophys 24:1–25

Richet P, Bottinga Y (1995) Rheology and configurational entropy of silicate melts. In: Stebbins JF, McMillan PF, Dingwell DB (eds) Structure, dynamics and properties of silicate melts. Mineralogical Society of America, Washington DC, pp 67–93

Richet P, Bottinga Y, Tequi C (1984) Heat capacity of sodium silicate liquids. J Am Ceram Soc 67:C6-C8

Risbud SH, Kirkpatrick RJ, Taglialavore AP, Montez B (1987) Solid-state NMR evidence of 4-, 5-, and 6-fold aluminum sites in roller-quenched SiO_2-Al_2O_3 glasses. J Am Ceram Soc 70:C10-C12

Robie RA, Hemingway BS (1995) Thermodynamic properties of minerals and related substances at 298.15 K and 1 bar (10^5 Pascals) pressure and at higher temperatures. US Geol Surv Bull 2131

Sato RK, McMillan PF, Dennison P, Dupree R (1991a) High resolution ^{27}Al and ^{29}Si MAS NMR investigation of SiO_2-Al_2O_3 glasses. J Phys Chem 95:4484

Sato RK, McMillan PF, Dennison P, Dupree R (1991b) A structural investigation of high alumina content glasses in the CaO-Al_2O_3-SiO_2 system via Raman and MAS NMR. Phys Chem Glasses 32:149–154

Stebbins JF (1987) Identification of multiple structural species in silicate glasses by ^{29}Si NMR. Nature 330:465–467

Stebbins JF (1988) Effects of temperature and composition on silicate glass structure and dynamics. J Non-Cryst Solids 106: 359–369

Stebbins JF (1995) Dynamics and structure of silicate and oxide melts: nuclear magnetic resonance studies. In: Stebbins JF, McMillan PF, Dingwell DB (eds) Structure, dynamics and properties of silicate melts. Mineralogical Society of America, Washington DC, pp 191–246

Stebbins JF, Carmichael ISE, Moret LK (1984) Heat capacities and entropies of silicate liquids and glasses. Contrib Mineral Petrol 86:131–148

Steele FN, Douglas RW (1965) The absorption of iron in silicate and borate glasses. Phys Chem Glasses 6:246–252

Stein DJ, Stebbins JF, Carmichael ISE (1986) Density of molten sodium aluminosilicates. J Am Ceram Soc 69:396–399

Tangeman JA (1998) Thermodynamic and transport properties of iron-bearing silicate melts. PhD Thesis, University of Michigan, 176 pp.

Taylor M, Brown GE (1979a) Structure of mineral glasses. I. The feldspar glasses, $NaAlSi_3O_8$, $KAlSi_3O_8$, $CaAl_2Si_2O_8$. Geochim Cosmochim Acta 43:61–77

Taylor M, Brown GE (1979b) Structure of mineral glasses. II. The SiO_2-$NaAlSiO_4$ join. Geochim Cosmochim Acta 43:1467–1473

Taylor M, Brown GE, Fenn PM (1980) Structure of mineral glasses. III. $NaAlSi_3O_8$ supercooled liquid at 805 °C and the effects of thermal history. Geochim Cosmochim Acta 44:109–119

Wang CM, Chen H (1987) Mixed coordination of Fe^{3+} and its dependence on the iron content in sodium disilicate glasses. Phys Chem Glasses 28:39–47

Wang Z, Cooney TF, Sharma SK (1993) High temperature structural investigation of $Na_2O.0.5Fe_2O_3.3SiO_2$ and $Na_2O.FeO.3SiO_2$ melts and glasses. Contrib Mineral Petrol 115:112–122

Wang Z, Cooney TF, Sharma SK (1995) In situ structural investigation of iron-containing silicate liquids and glasses. Geochim Cosmochim Acta 59:1571–1577

Wilson AD (1960) The micro-determination of ferrous iron in silicate minerals by a volumetric and a colorimetric method. Analyst 85:823–827